UV to NIR photon conversion in Nd-doped rutile and anatase titanium dioxide films for silicon solar cell application

E. Le Boulbar [a,*], E. Millon [a], E. Ntsoenzok [b], B. Hakim [b], W. Seiler [c], C. Boulmer-Leborgne [a], J. Perrière [d]

[a] GREMI, UMR 7344 CNRS – Université d'Orléans, BP 6744, 45067 Orléans Cedex 2, France
[b] CEMHTI, UPR 3079 CNRS, 1D avenue de la recherche scientifique, 45071 Orléans, France
[c] PIMM, UMR 8006 CNRS – ENSAM, 151 Boulevard de l'Hôpital, 75013 Paris, France
[d] INSP, UMR 7588 CNRS – Université Paris 6, 4 place Jussieu, 75005 Paris, France

A B S T R A C T

Undoped and Nd-doped titanium dioxide anatase and rutile films have been grown by pulsed-laser deposition at 700 °C under 0.1 mbar O_2. By selecting adequate substrates, TiO_2 films doped with 1, 2 or 5 at.% Nd were grown and constituted with polycrystalline rutile, highly oriented (2 0 0) rutile film, or oriented (0 0 4) anatase. An UV to NIR photon conversion is evidenced in the films. Indeed, intense and well-resolved emission lines from Nd^{3+} have been observed upon excitation above the TiO_2 bandgap at room temperature. The sensitised emission of Nd^{3+} is found to be much efficient in rutile than in anatase structure. Low temperature photoluminescence measurements lead to fine resolved peaks corresponding to the Nd^{3+} 4f transitions with different spectral characteristic according to the host matrix used. Photoluminescence dependence temperature evidences that the light emission from Nd^{3+} in anatase-based films is probably influenced by the presence of self-trapped excitons or by orbital interaction. Mechanisms of sensitisation host to Nd^{3+} are proposed for both matrixes. Finally, the Nd dopant concentration and the microstructure of TiO_2 rutile films are found to affect the photoluminescence emission intensity. Rutile film (2 0 0) oriented is the most adapted host matrix to sensitise 1 at.% Nd^{3+} ions for an emission around 1064 nm making such Nd-doped layers interesting for photon conversion by down shifting process.

1. Introduction

The best single crystal silicon solar cell efficiency reaches a maximum of 24.7% [1] close to the limit of 31% calculated by Shockley and Queisser [2]. One of the origins of this limited efficiency is related to the spectral mismatch: photons with energy smaller than the band-gap are not absorbed (sub-band-gap transmission) and a large part of the energy of photons with energy larger than the band gap is lost as heat (thermalization losses). Photon management is one of the third generation photovoltaic principles which can lead to the improvement of silicon solar cell yield [3]. High energy photon might be split in one or two photons with a smaller energy. Each of these photons can subsequently be absorbed by the solar cell and generate an electron–hole pair. These processes, known as down-shifting (DS) for one emitted photon or down-conversion (DC) for two emitted photons, are beneficial for solar cells with a smaller band-gap where thermalization losses are the major loss factor. Lanthanides ions are fitted to DS or DC purpose as their atomic energy levels allow efficient spectral

conversion. DC of UV or visible photons into more than one NIR photons with lanthanides ions was first demonstrated in Y, $YbPO_4:Tb^{3+}$ [4]. After excitation into the $^5D_4$ state of the Tb^{3+} ion, two neighbouring Yb^{3+} ions are excited through a cooperative energy transfer process. The $^5D_4$ level of Tb^{3+} is about twice the energy of the Yb^{3+} $^2F_{5/2}$ level, and after energy transfer Yb^{3+} emission is observed around 1000 nm. This emission is just above the band gap of crystalline silicon which makes Yb^{3+} an attractive candidate for DC materials to be used in combination with silicon solar cells. More recently, cooperative DC has also been reported for Tb^{3+}/Yb^{3+} in other host materials and with other lanthanide couples Pr^{3+}/Yb^{3+}; Tm^{3+}/Yb^{3+} and Nd^{3+}/Yb^{3+} [5–12]. Rare earth ion couples seems to be adequate for UV to NIR photons conversion as theoretical and experimental calculation of external quantum efficiency have reached more than 100% efficiency [9]. Nevertheless, these promising results on DC with lanthanides do not hide remaining challenge. Indeed, the absorption strength of 4f–4f transition is very weak and limited to narrow lines, which does not allow absorption of a large part of solar cell spectrum. To solve the absorption problem a third ion or a host matrix is required to work as a sensitizer which could absorbed efficiently all light in the UV and visible part of the spectrum up to ~500 nm and then transfer energy to the DC couple, e.g. the $^3P_0$ level of Pr^{3+} [9].

* Corresponding author.
  E-mail addresses: emmanuel.leboulbar@gmail.com, E.Le.Boulbar@bath.ac.uk (E. Le Boulbar).

Richards [13] pointed out that TiO_2 should be an interesting matrix to host rare earth ions because of its high-refractive index, and its excellent transparency to visible/NIR light. Besides, Nd^{3+} ion is of particular interest for energy transfer as it has plenty of high energy level suitable to overlap TiO_2 conduction band and $^4F_{3/2} \rightarrow {}^4I_J$ transitions are just above silicon energy band gap. In most reported cases, selected matrix is anatase and no work has been focused on structure and microstructure in relation with energy transfer efficiency and mechanisms. Since anatase (tetragonal, space group I4$_1$/amd (No. 141), lattice parameters: $a = b = 0.378$ nm and $c = 0.951$ nm) and rutile (tetragonal, space group P4$_2$/mnm (No. 136), lattice parameters: $a = b = 0.459$ nm and $c = 0.296$ nm) display different structural and optical properties as well as different phonon energy ($h\nu_{max}$ is 650 and 815 cm^{-1}, respectively [14–16]) the TiO_2 host matrix might affect Ln^{3+} luminescence and transfer properties. In the same way, the structural properties (crystallinity, grain size, crystallite orientation in films) might infer particular luminescence emission.

In this paper, the photoluminescence (PL) properties of Nd^{3+} have been recorded upon excitation of TiO_2 band gap in order to investigate matrix to Nd energy transfer and the related effect of the structural properties of the TiO_2 host matrix. At this aim, the crystallinity and the main axis growth of TiO_2 anatase or rutile films have been controlled by using the pulsed-laser deposition (PLD) method which is well-adapted to growth high crystalline quality thin films with complex composition. Indeed, the nature of TiO_2 phases and their main axis growth can be adjusted by choosing appropriate substrates as LaAlO$_3$ (1 0 0) (rhombohedral at room temperature and usually defined as hexagonal, space group R-3c (No. 167), lattice parameters: $a = 0.536$ nm, $c = 1.311$ nm. It can also be represented as pseudocubic with $a = 0.3793$ nm), Al$_2$O$_3$ (0 0 0 1) (hexagonal, space group R-3c (No. 167), lattice parameters: $a = 0.475$ nm, $c = 1.298$ nm.), or silicon substrate [17–19]. Host-sensitised $TiO_2:Nd^{3+}$ energy transfer has been therefore recorded in both anatase (labelled A-TiO$_2$ in this paper) and rutile (R-TiO$_2$) films with various structural properties. The Nd^{3+} surrounding and the energy transfer from the TiO_2 matrixes to Nd^{3+} ions are analysed and the effects of the matrix and the Nd^{3+} doping content are evidenced. Finally, the integrated PL intensity recorded on R-TiO$_2$ films is discussed according to the microstructure of films (polycrystalline or oriented).

2. Experimental section

PLD is a method particularly adapted for the growth of complex oxide films [20,21]. TiO_2 thin films doped Nd^{3+} were grown by PLD with a KrF Lambda Physics Compex 201 laser (248 nm, 27 ns, 20 Hz pulses). The experimental set-up was described elsewhere [22]. Depositions were performed on 10 mm × 10 mm × 0.5 mm single crystal Al$_2$O$_3$ (0 0 0 1), LaAlO$_3$ (1 0 0) or Si (1 0 0) substrates. The laser was focused onto the target with a fluence of 4 J cm^{-2}. The incident angle of the beam to the rotating target surface was fixed at 45°. Homemade one inch titanium oxide targets with 1.0, 2.0 or 5.0 at.% Nd-doped concentration were used for the experiments. The substrate to target distance was set to 4.5 cm along the normal from the target. Ultra-pure oxygen was introduced into the vacuum chamber with a mass flow controller to maintain the desired partial pressure (10^{-1} mbar). Substrates were silver pasted onto the heater substrate holder parallel to the target. Substrates were heated to the desired growth temperature ($T_s = 700$ °C) and held at growth temperature for 10 min both before and after the deposition.

The thickness and composition of the titanium oxide films were measured by Rutherford backscattering spectrometry (RBS), using a 2 MeV energy $^4He^{2+}$ ion beams from the Van de Graaff accelerator of the SAFIR IBA Laboratory, Université Pierre et Marie Curie, Paris, France. The precise determination of the in-depth distribution of the elements of films and substrates was obtained by the RUMP simulation program. Such an analysis provides the titanium and oxygen concentrations in the films with a relative precision close to 4%, mainly due to the low RBS yield on oxygen. Moreover, this RBS analysis demonstrates the absence of interdiffusion between the titanium oxide phases and the substrates (whatever the nature and orientation of the single crystal substrate) despite growth performed at relatively high temperature (700 °C). The structural characterizations of the titanium oxide films were carried out by X-ray diffraction (XRD) analyses using a four circle diffractometer (Philips Xpert MRD) with the CuKα radiation ($\lambda = 0.154$ nm). The nature of the crystalline phases, their axes parameters and their eventual preferential orientations with respect to the substrates were investigated in the symmetric Bragg–Brentano geometry.

Optical transmission measurements were performed on undoped rutile and anatase films or doped with Nd^{3+} at contents of 1.0%, 2.0% and 5.0% grown on both side polished LaAlO$_3$ (1 0 0) and sapphire substrates using a spectrophotometer Jasco UV–Visible V-530, with a resolution of 2 nm, in 300–1000 nm wavelength range. Spectrum transmission were corrected from LaAlO$_3$ (1 0 0) and sapphire substrate absorption for all samples.

Photoluminescence emission spectra were recorded upon an UV excitation at $\lambda = 364$ nm provided by a Spectra Physics argon laser. Jobin–Yvon iHR320 spectrometer composed of a Cnerzy–Turner monochromator and an InGaAs sensor were used to record photoluminescence intensity with respect to wavelength. Spectral resolution was set to the limit of our equipment, i.e. 0.5 nm for each step. Photoluminescence spectra were normalised according to films thickness.

3. Results and discussion

3.1. Samples composition, crystalline structure and optical properties

The RBS experiments evidences that the films are nearly stoichiometric as an O/Ti ratio equal to 2 is measured on the films whatever the substrate used. Such composition is classically observed on titanium oxide film grown under oxygen pressure (0.1 mbar). According to RBS measurements, the concentration of Nd^{3+} in the TiO_2 films reaches 1.0, 2.0 or 5.0 at.%.

The structural properties have been investigated by XRD on undoped and Nd-doped TiO_2 films on the different substrates. Fig. 1 shows the XRD patterns of undoped TiO_2 films. On LaAlO$_3$ (1 0 0) substrate, the peak located at $2\theta = 37.80°$, corresponds to a film with the anatase single phase oriented according to the (0 0 4) plane parallel to the surface substrate (such film is labelled A$_{004}$). The growth of TiO_2 films on both Al$_2$O$_3$ (0 0 0 1) substrate show a main peak at $2\theta = 39.18°$, which is related to the growth of rutile (2 0 0) (R$_{200}$) oriented film, respectively. The diffraction peaks of films grown on Si (1 0 0) substrate can be indexed as the polycrystalline rutile phase (here labelled R$_{PC}$). For TiO_2 films doped by Nd^{3+}, the XRD diagrams are very similar (the same phases and orientations are observed) and no peak related to other impurity phases such as neodymium oxides, or neodymium titanium oxides are observed. Inserted Nd ion into rutile and anatase matrixes does not modify 2θ position and fwhm (2 0 0) and (0 0 4) peaks.

UV–Visible transmission spectra of undoped and Nd-doped A$_{004}$ and R$_{200}$ thin films are shown in Fig. 2. Doping rutile and anatase do not modify the 95% and 85% visible transparency of A$_{004}$ and R$_{200}$ samples. The bandgap energy (E_g) of the undoped and Nd-doped A$_{004}$ and R$_{200}$ films determined from the Tauc plot are listed in Table 1. The bandgap energies of undoped A$_{004}$ and R$_{200}$ were determined to be 3.07 eV and 3.17 eV, respectively. These values
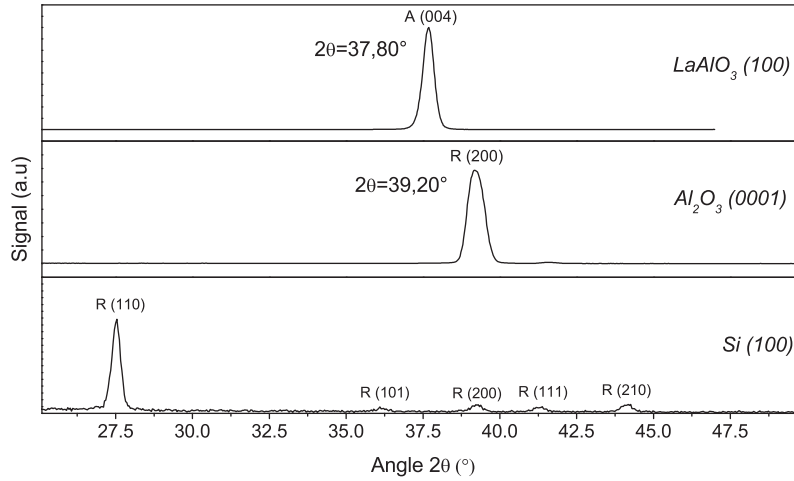
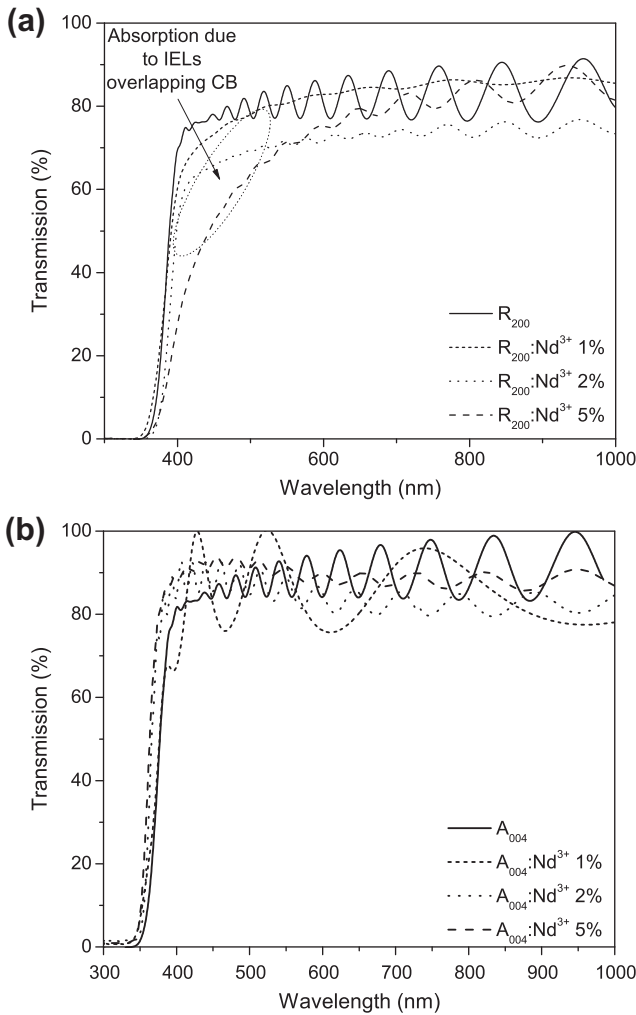**Fig. 1.** XRD patterns of TiO$_2$ thin films grown on Al$_2$O$_3$ (0 0 0 1), LaAlO$_3$ (1 0 0) and Si (1 0 0) substrates.

Fig. 2. Transmission spectra of: (a) R$_{200}$:Nd^{3+} and (b) A$_{004}$:Nd^{3+}.

Table 1
Optical band gap of R$_{200}$ and A$_{004}$ films doped with 0, 1, 2 and 5 at.% in Nd^{3+}.

Nd^{3+} doping (%)	0	1	2	5
R$_{200}$	3.07	3.10	3.02	2.97
A$_{004}$	3.17	3.27	3.28	3.30

increasing Nd^{3+} content results in a biggest absorption appeared between 400 and 550 nm only in R$_{200}$ sample (Fig. 2), and particularly for 5% R$_{200}$:Nd^{3+}. This behaviour might be explained by the overlap of impurity energy levels (IELs) appearing just below the conduction band [24].

3.2. Energy transfer in host sensitised Nd^{3+} doped rutile and anatase TiO$_2$

The PL spectra under UV excitation ($\lambda = 364$ nm) of R- and A-TiO$_2$ films doped with 1 at.% Nd^{3+} are represented in Fig. 3. Radiative desexcitation from level $^4F_{3/2}$ to ^4I_J ($J = 9/2$, 11/2, 13/2) of Nd^{3+} gives rise to three groups of peaks centred at 900, 1100 and 1350 nm wavelengths in agreement with the emission levels involved for Nd^{3+} ion (Fig. 4). This emission pattern is very different from that of Nd^{3+} in Nd$_2$O$_3$ for both peak position and line shape,
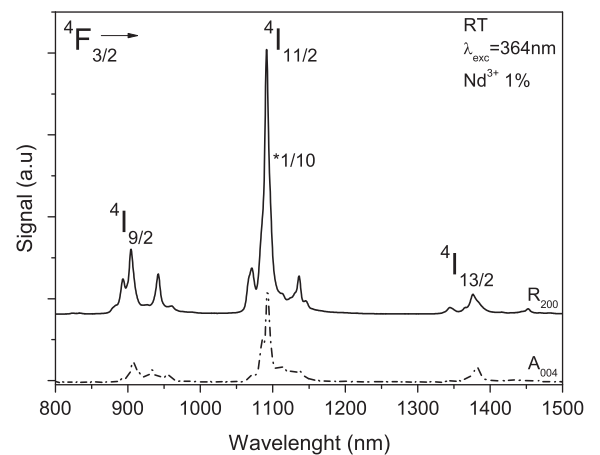

Fig. 3. Room temperature emission spectra under excitation at 364 nm of 1% Nd^{3+}-doped anatase and rutile thin films. The real intensity of PL spectrum of Nd^{3+}-doped R$_{200}$ is 10 times greater.

are lower than those of generally observed in anatase and rutile films (3.4 and 3.3 eV, respectively [23]). The optical band gap extracted by Tauc plot method shows a redshift for the R$_{200}$:Nd^{3+} films from 3.07 to 2.97 eV while the reverse effect is observed for the A$_{004}$:Nd^{3+} films (blueshift, from 3.17 to 3.30 eV). Moreover,
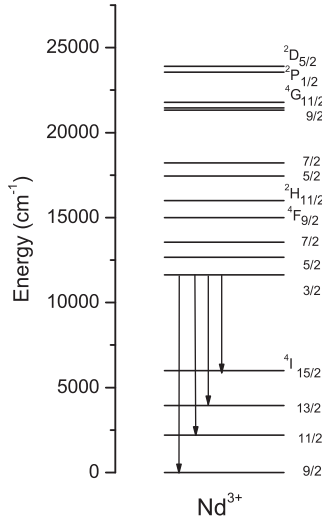
Fig. 4. Energy diagram of Nd^{3+} ion [26].

and thus the presence of Nd_2O_3 in the synthesised films is excluded. Low temperature PL measurements have been carried out in order to evaluate Nd^{3+} local environment in R-TiO_2 (Fig. 5) and A-TiO_2 (Fig. 6). A marked decrease in the width of individual crystal-field-split spectral lines appeared as the temperature is lowered. In addition, some spectral lines are absent at 10 K and appear only as the temperature increases (indicated by arrows in Figs. 5 and 6). As spectral lines become thinner due to the absence of thermal broadening, $^4F_{3/2} \rightarrow {}^4I_{9/2}$, $^4F_{3/2} \rightarrow {}^4I_{11/2}$ and $^4F_{3/2} \rightarrow {}^4I_{13/2}$ transitions in Nd^{3+} doped R_{200} and A_{004} can be well determined and are respectively centred at 904 (907), 1091 (1093) and 1376 (1382) nm. Similar shifts between peak positions have been recorded [25] for TiO_2:Sm^{3+} ions and has been explained by the slight difference between Ln^{3+} surrounding local environments. Indeed, crystal field is not equivalent in TiO_2 matrixes and can be described as D_{2d} symmetry of the neodymium position in anatase, whereas D_{2h} provides an accurate description for rutile environment, as shown for Sm^{3+}

[25]. The PL measurements indicate that the neodymium position in the crystal network might also be described by lower symmetry for the Nd^{3+} ion in rutile.

For PL recorded at room temperature with the same experimental conditions, it is surprising to notice that R_{200}:Nd^{3+} line spectrum is much more intense than A_{004}:Nd^{3+} one (Fig. 3), considering anatase and rutile phonon cut-off characteristics. Note that in Fig. 3, the signal related to R_{200}:Nd^{3+} is divided by 10 for comparison purpose. The integrated PL intensity from 800 to 1500 nm is 30 times larger in R_{200}:Nd^{3+} than in A_{004}:Nd^{3+} for 1% Nd^{3+} doped samples. A quenching effect is highly improbable as it dominates generally at dopant concentration up to 2% [25]. This difference highlights a relevant feature in energy transfer efficiency and might be explained by different host-to-Ln^{3+} energy transfer pathway.

As anatase matrix has a lower cut-off phonon frequency than for rutile matrix, much intense PL spectral lines should be provided by Nd^{3+} ions introduced in A-TiO_2 rather than in R-TiO_2 matrix. Indeed, higher the phonon cut-off frequency is, higher the probability of non-radiative multiphonon transfer would be. The minimum number of phonon p required for a transition from 4f state splits by an energy difference ΔE in a matrix where the phonon cut off frequency is v_{max} is given by the following equation:

$$p = \frac{2\pi \times \Delta E}{h \times v_{max}}$$

Empirically, multiphonon non-radiative transfer is a predominant process when energy is less than 5–6 cut-off phonon energy [26]. Following that empirical rule also known as gap law, a dominance of multiphonon relaxation process is predicted for all $\Delta E < 3900$ cm^{-1} and 4880 cm^{-1} for anatase and rutile, respectively. According to Dieke diagram [27], multiphonon process should occur for Nd^{3+} in anatase and rutile matrixes for all high energy states to $^4F_{3/2}$ transitions but not for $^4F_{3/2} \rightarrow {}^4I_J$ transitions as ΔE is bigger than 6000 cm^{-1}.

Fig. 7 illustrates possible mechanisms for the host-to-Nd^{3+} sensitisation in R_{200} and A_{004} films. The excitation above the bandgap of titania films leads to the transition of electrons in TiO_2 bulk from valence band (VB) to conduction band (CB) leaving holes in VB. It is believed that the energy of a recombination of electron–hole
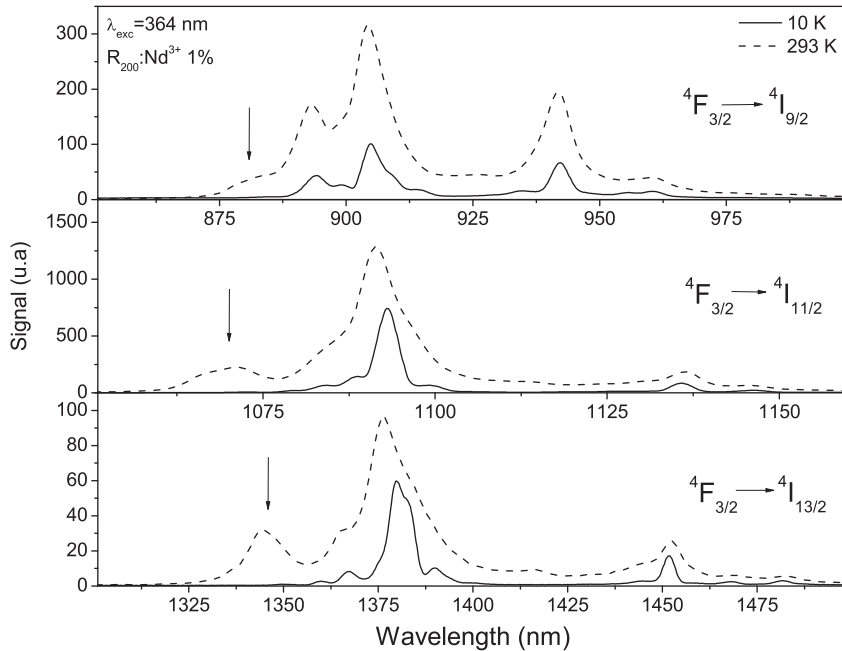

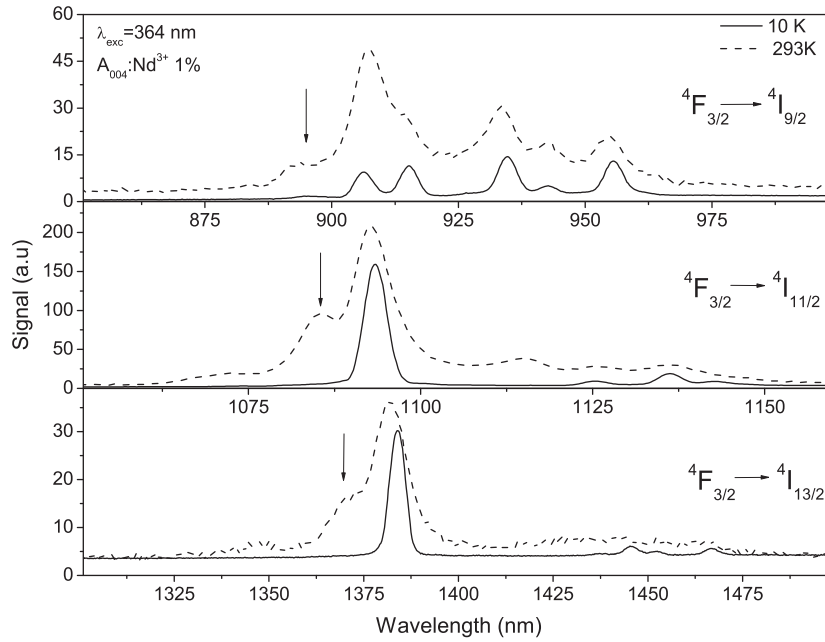**Fig. 5.** 10 K and room temperature PL of 1% Nd^{3+}-doped R_{200} film.

Fig. 6. 10 K and room temperature PL of 1% Nd^{3+}-doped A_{004} film.
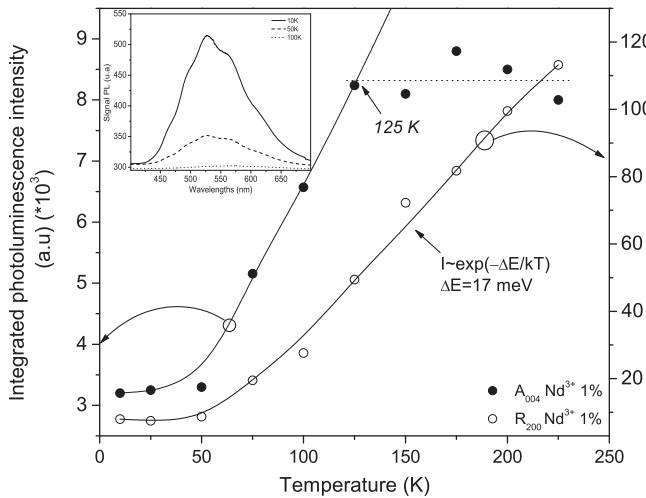

Fig. 7. Integrated PL intensity of Nd^{3+} signals as a function of temperature in 1% Nd^{3+} doped anatase and rutile films. The inset shows the self-trapped exciton luminescence peak for three temperatures: 10 K (full line), 50 K (bold dotted line), and 100 K (dotted line).

may appear competitive energy transfer processes from A-TiO$_2$ CB to self-trapped exciton (STE) defects and Nd^{3+} energy states A-TiO$_2$. Indeed, overall intensity for Nd^{3+}-doped rutile film as a function of temperature shows an exponential behaviour instead that of A_{004}:Nd^{3+} film exhibits first an exponential behaviour until 125 K and then followed by a linear slope (Fig. 8). The apparition of this break can be linked to the quenching of self-trapped excitation, seen in Fig. 7 and reported in the literature at 180 K [28]. Such host sensitisation may be ascribed to a phonon-assisted energy transfer process since relatively weak host-to-Ln^{3+} sensitisation were observed at 10 K and as the signal is improved when the temperature increases. After the energy transfer from CB to Nd^{3+} excited state, non-radiative relaxation to $^4F_{3/2}$ of Nd^{3+} occurs thanks to multiphonon relaxation, then $^4F_{3/2} \rightarrow {}^4I_J$ producing near-infrared emissions (Fig. 8).

generated in the host can transfer non-radiatively to the excited states of Nd^{3+} ions for both matrixes. The first difference might be a much efficient CB to Nd^{3+} excited level in R-TiO$_2$:Nd^{3+}. Indeed, as the phonon cut-off frequency is stronger in R-TiO$_2$ than in A-TiO$_2$, the energy transfer from CB to Nd^{3+} neighbouring excited state (possibly the $^4D_{1/2}$ state of Nd^{3+}) might be enhanced in rutile. Moreover, the efficiency of CB to Nd^{3+} energy transfer in R-TiO$_2$ might be explained by the relevant hybridizing of Nd 4f with O 2p orbital observed in R-TiO$_2$:Nd^{3+} which does not occurred in Nd^{3+}-doped anatase. Indeed, it is well known that the most efficient energy transfer process involves resonance between the sensitizer and activator transition and are observed when there is an overlap of the sensitizer band and the acceptor band. Moreover, low temperature PL measurements on anatase samples showed a broad peak, that is a characteristic of self-trapped exciton (STE) defects (inset Fig. 7). Due to the presence of this defect, it
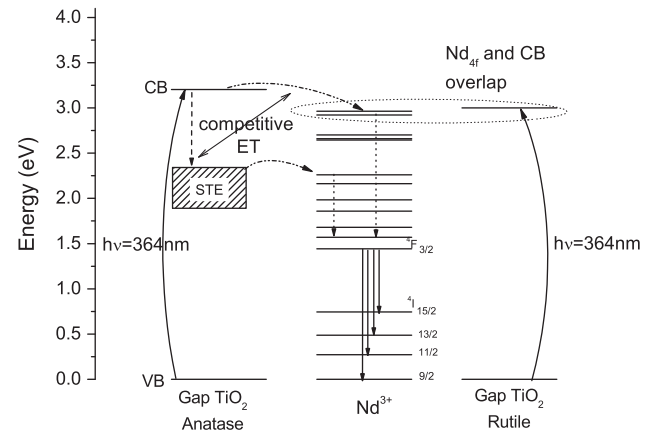

Fig. 8. Energy transfer mechanism describing competitive transfer and Nd^{3+} sensitisation in A-TiO$_2$ and R-TiO$_2$. One UV-blue photon absorbed by a Nd^{3+} ion is converted to one Nd^{3+} NIR photons through a two-step sequential energy transfer. Solid, curved dotted, and straight arrows represent optical transition, non-radiative energy transfer, and non-radiative relaxation.

3.3. Effect of dopant concentration on integrated photoluminescence intensity

Room temperature integrated PL intensities of 1%, 2% and 5% Nd^{3+}-doped TiO_2 films have been calculated in order to investigate the influence of the dopant concentration. As shown in Fig. 9a, an increase of Nd^{3+} concentration from 1 to 5 at.% leads to increase gradually the total PL intensity for both structures. Normalised integrated signal gives rise to information about quenching, showing that Nd^{3+} ion luminescence efficiency is decreased by increasing dopant content (Fig. 9b). Normalised overall intensity of R_{200}:Nd^{3+} by the doping content gives an access to emission efficiency of each Ln^{3+} ions. The signal corresponding to 2 or 5 at.% Nd is divided by two and three referring to the lowest doping content (1%) which means that the decrease of efficiency can be assigned to a quenching effect. Indeed, the cross-relaxation rate critically depends on the distance between the Ln^{3+} pairs (i.e., Ln^{3+} concentrations). For Nd^{3+} ions, it exists the following cross-relaxation dipolar transition: the energy produced by the $^4F_{3/2} \rightarrow ^4I_{15/2}$ transition of one Nd^{3+} ion can be resonantly transferred to another neighbouring Nd^{3+} ion causing the $^4I_{9/2} \rightarrow ^4I_{15/2}$ excitation. The electrons in the $^4I_{15/2}$ excited state are non-radiatively relaxed to the $^4I_{9/2}$ fundamental state. It has been observed in anatase nanocrystal, that cross relaxation occurs at
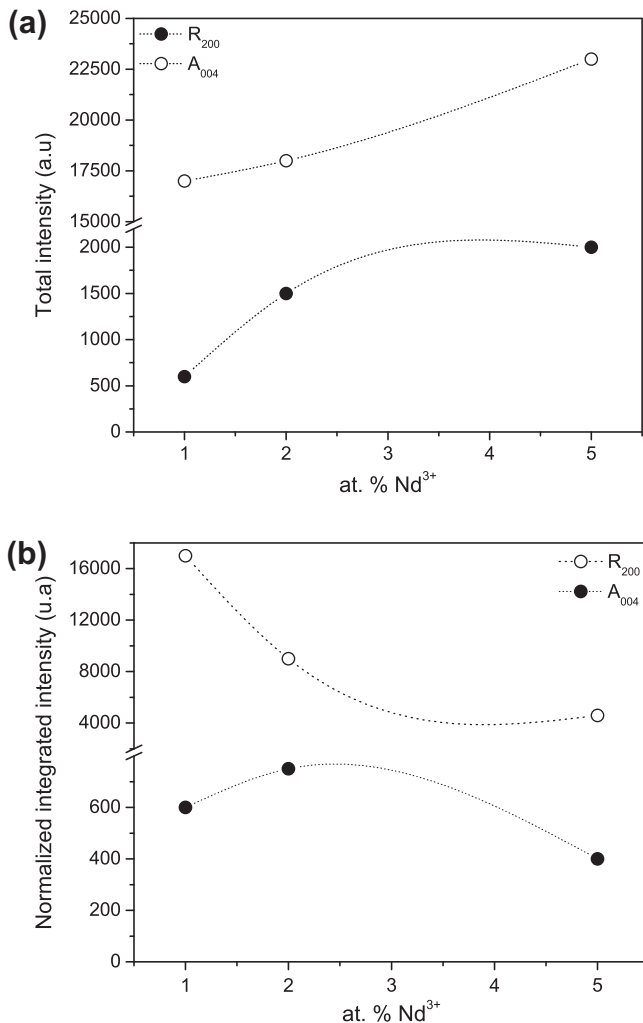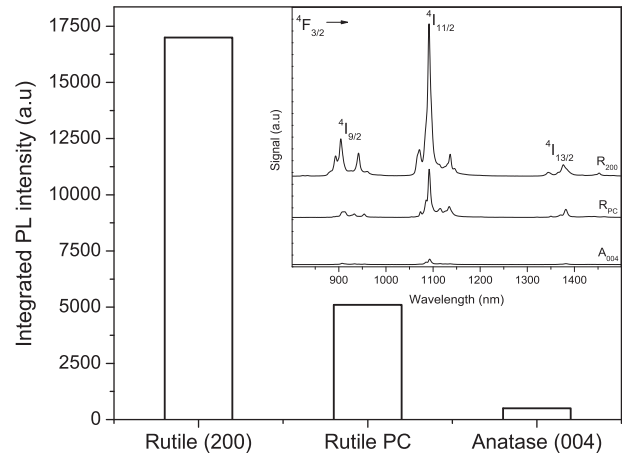

Fig. 10. UV excited room temperature integrated luminescence of 1% Nd^{3+} doped R_{200}, R_{PC} and A_{004} samples. Characteristics Nd^{3+} $^4F_{3/2}$ ^4I_J transitions obtained in each TiO_2 film are represented in insert.

Table 2
Full width half maximum of TiO_2 films and relative grain size diameter calculated by the Scherrer equation.

Films	2θ (°)	Phase	FWHM (°)	$D_{Scherrer}$ (nm)
R_{200}	39.20	R-TiO_2 (2 0 0)	0.33	26
A_{004}	37.80	A-TiO_2 (0 0 4)	0.43	20
R_{PC}	27.50	R-TiO_2 (PC)	0.32	28

all dopant concentration and the PL signal is quenched dramatically when the amount of Nd^{3+} dopant was increased up to 2% [5]. These drops are attributed to the enhancement of cross relaxation process due to higher concentration. It has to be noticed that the luminescence efficiency of Nd^{3+} ion decreases for higher Nd concentration, but the extinction of luminescence is not observed.

3.4. Effect of rutile microstructure on integrated photoluminescence intensity

Fig. 10 shows the integrated emission intensities from 800 to 1500 nm of R_{200}, R_{PC} and A_{004} films doped by 1 at.% Nd^{3+}. A_{004} has the smallest amount of integrated luminescence making anatase a non-suitable host-matrix for Nd^{3+} ions. The effect of rutile microstructure is investigated by taking into account XRD peaks, as it is related to the grain size of crystallites and localised strains inside the films (Table 2). It is interesting to notice that R_{200} shows twice larger integrated PL signal than R_{PC} films. Regarding XRD patterns, these differences could be explained by a better crystalline quality in R_{200} rather than in R_{PC} as the FWHM of (2 0 0) peak of R-TiO_2 is smaller than the other ones. In previous works [17,18], it has been demonstrated that R- or A-TiO_2 films grown on sapphire and $LaAlO_3$ substrates are strongly oriented according to the same out-of plane relationships evidenced in the present study and they are also epitaxied allowing for such films to be almost considered as like-single crystal. Despite its interesting structural properties, the A-TiO_2 films do not lead to intense PL emission due to the STE process. Consequently, the R_{200} film displays the best structural properties in terms of grain size, density, and quality of film/substrate interface. The PL properties of this film are therefore more efficient than those of induced from a polycrystalline rutile film which is characterised by a higher structural disorder.

Fig. 9. Integrated (a) and normalised (b) PL intensity in the 800–1500 nm range corresponding to the $^4F_{3/2} \rightarrow ^4I_J$ Nd^{3+} transition for 1%, 2% and 5% Nd^{3+}-doped A_{004} and R_{200} films.

4. Conclusion

Undoped and Nd-doped rutile and anatase TiO_2 thin films have been successfully grown by pulsed laser deposition under 10^{-1} mbar at 700 °C. The nature of phase (A or R) and its main axis growth may be controlled thanks to the substrate used. Different Nd^{3+} doping contents have been obtained: 1, 2 and 5 at.%. The photoluminescence of the obtained UV host-sensitised Nd^{3+} has been realised upon excitation of the rutile and anatase matrix. A slight difference is observed in the fine structure of the PL spectrum shape between A-TiO_2 and R-TiO_2 oriented with the (0 0 4) and (2 0 0) planes parallel to surface substrate, respectively. That suggests different Nd^{3+} local environment in the host crystal field. These differences, highlighted by the modification of rutile absorption spectrum, would induce that interactions between Nd^{3+} ions and TiO_2 network are stronger in the rutile phase. The host-sensitisation may occur according to a phonon assisted energy transfer as the PL peak intensities in the two matrixes are growing up with respect to temperature. Nevertheless, energy transfer is found to be different in both matrixes: the transfer from rutile to Nd^{3+} ions is much efficient, probably both due to the O 2p and Nd^{3+} 4f hybridization while a competitive transfer involving self-trapped excitons occurs in anatase. Finally, we demonstrate that UV to NIR conversion is achieved in both anatase and rutile phase and that high crystalline quality rutile film is the most efficient matrix to host Nd^{3+} ions leading to the most efficient PL emission. Such Nd^{3+}-doped rutile films are now studied as potential upper layer on silicon solar cell toward a possible improvement of the photon conversion efficiency based on a UV to NIR down shifting process.

References

[1] J. Zhao, A. Wanh, M.A. Green, Prog. Photovolt.: Res. Appl. 7 (6) (1999) 471–474.
[2] W. Shockley, H.J. Queisser, J. Appl. Phys. 32 (3) (1961) 510–519.
[3] G. Conibeer, Mater. Today 10 (11) (2007) 42–50.
[4] P. Vergeer, T.J.H. Vlugt, M.H.F. Kox, M.I. den Hertog, J.P.J.M. van der Eerden, A. Meijerink, Phys. Rev. B 71 (2005) 014119.
[5] G. Lakshminarayana, Y. Hucheng, Y. Song, L. Yin, Q. Jianrong, J. Phys. D: Appl. Phys. 41 (2008) 175111.
[6] G. Lakshminarayana, J. Qiu, J. Alloys Compd. 481 (2009) 582–589.
[7] L. Aarts, B.M. van der Ende, A. Meijerink, J. Appl. Phys. 106 (2009) 023522-6.
[8] J.-M. Meijer, L. Aarts, B.M. van der Ende, T.J.H. Vlugt, A. Meijerink, Phys. Rev. B 81 (2010) 035107.
[9] B.M. Van der Ende, L. Aarts, A. Meijerink, Phys. Chem. Chem. Phys. 11 (2009) 11081–11095.
[10] H. Lin, D. Chen, Y. Yu, Z. Shan, P. Huang, A. Yang, Y. Wang, J. Alloys Compd. 509 (2011) 3363–3366.
[11] Q.Y. Zhang, C.H. Yang, Z.H. Jiang, X.H. Ji, Appl. Phys. Lett. 90 (2007) 061914-3.
[12] Q.Y. Zhang, G.F. Yang, Z.H. Jiang, Appl. Phys. Lett. 91 (2007) 051903.
[13] B.S. Richards, Solar Energy Mater. Solar Cells 90 (2006) 1189–1207.
[14] F. Jing, S. Harako, S. Komuro, X. Zhao, J. Phys. D: Appl. Phys. 42 (2009) 085109.
[15] S.P.S. Porto, P.A. Fleury, T.C. Damen, Phys. Rev. 154 (1967) 522.
[16] M. Montagna, E. Moser, F. Visintainer, M. Ferrari, L. Zampedri, A. Martucci, M. Guglielmi, M. Ivanda, J. Sol–Gel Sci. Technol. 26 (2003) 241–244.
[17] N. Sbaï, J. Perrière, W. Seiler, E. Millon, Surf. Sci. 601 (2007) 5649–5658.
[18] N. Sbaï, J. Perrière, B. Gallas, E. Millon, W. Seiler, M.C. Bernard, J. Appl. Phys. 104 (2008).
[19] S. Yamamoto, T. Sumita, Sugiharuto, A. Miyashita, H. Naramoto, Thin Solid Films 401 (2001) 88–93.
[20] A. Roemer, E. Millon, B. Vincent, A. Boudrioua, O. Pons-Y-Moll, R.M. Defourneau, W. Seiler, J. Appl. Phys. 95 (2004) 3041–3047.
[21] P.A. Atanasov, R.I. Tomov, J. Perrière, R.W. Eason, N. Vainos, R. Kliny, A. Zherikhin, E. Millon, Appl. Phys. Lett. 76 (2000) 2490–2492.
[22] E. Le Boulbar, E. Millon, J. Mathias, C. Boulmer-Leborgne, M. Nistor, F. Gherendi, N. Sbaï, J.B. Quoirin, Appl. Surf. Sci. 257 (2011) 5380–5383.
[23] H. Gudel, M. Pollnau, J. Alloys Compd. 303–304 (2000) 5317–5323.
[24] Z. Zhao, Q. Liu, J. Phys. D: Appl. Phys. 41 (2008) 085417.
[25] W.Q. Luo, R.F. Li, X.Y. Chen, J. Phys. Chem. C 113 (2009) 8772–8777.
[26] J.M. Van Dijk, M.F.H. Schuurmans, J. Chem. Phys. 78 (1983) 5317–5323.
[27] R.T. Wegh, A. Meijerink, R.J. Lamminmaki, J. Holsa, J. Lumin. 87–89 (2000) 1002–1004.
[28] V. Melnyk, V. Shymanovska, G. Puchkovska, T. Bezrodna, G. Klishevich, J. Mol. Struct. 573 (2005) 744–747.